

# Results from the 2009 campaign on WR 140

Peredur Williams

Institute for Astronomy, Royal Observatory, Edinburgh, UK

**Abstract:** The archetypal Wolf-Rayet + O star colliding-wind binary WR 140 has a very elliptical orbit, so that maximum interaction between the WR and O winds, and the most rapid changes in configuration, occur around periastron passage. To exploit this laboratory for studying wind-collision and high-energy phenomena, several groups mounted campaigns to observe WR 140 intensively around the most recent (2009) periastron passage. These included multi-site optical spectroscopy to refine the radial velocity orbit and study anomalous emission from the shock-compressed wind, infrared spectroscopy to study related features and map the wind-collision region, high-resolution radio imaging of the wind-collision shock, and X-ray observations with *RXTE*, *XMM-Newton*, *Chandra* and *Suzaku* to study physical conditions in the shocks. Some preliminary results from these campaigns will be surveyed and the synergy of multi-wavelength observations considered.

## 1 Context: A multi-wavelength history of WR 140

The WC7+O5 Wolf-Rayet system WR 140 (HD 193793, BD +43°3571; all three designations are used at different times in the literature but, for simplicity, only the first will be used here despite the anachronisms) is the archetypal WR colliding-wind binary (CWB). It shows anomalously strong X-ray emission, non-thermal radio emission, infrared emission from condensation of carbon dust and conspicuous variation of spectral line profiles. These phenomena all vary round the  $P \simeq 8$ -year binary orbit, partly because of our changing viewing angle, but mostly because the orbit of WR 140 is very elliptical ( $e > 0.88$ ), so that the interaction of the stellar winds varies hugely as the separation of the stars varies by a factor of  $\sim 18$  round the orbit. The high eccentricity of the orbit may have contributed to the delay in recognition of WR 140 as a binary. On the basis of nine discordant radial velocities (RVs) measured in 1921–22, Plaskett (1924) suggested that WR 140 was a spectroscopic binary but, although many more RVs were measured in subsequent studies over six decades, no RV orbit was found (e.g. McDonald 1947, Conti et al. 1984). It was the observation of a second dust-formation episode in the infrared that allowed Williams et al. (1987) to suggest a period (7.9 y.) for these events and demonstrate that the RVs could be fit with a high-eccentricity orbit having the same period and going through periastron passage shortly before dust formation. This was probably the first, but certainly not the last, instance of multi-wavelength synergy in the study of CWBs. The multi-wavelength infrared photometry continued, and a long-term light curve in  $L'$  ( $3.8\mu\text{m}$ ) is shown in Fig. 1.

Another wavelength region where WR 140 showed unexpected behaviour was in the radio. In 1975, Florkowski & Gottesman (1977) observed radio emission having a spectrum,  $S_\nu \propto \nu^{-0.2}$ , which differed from that expected from a stellar wind, suggesting variable mass loss. The emission

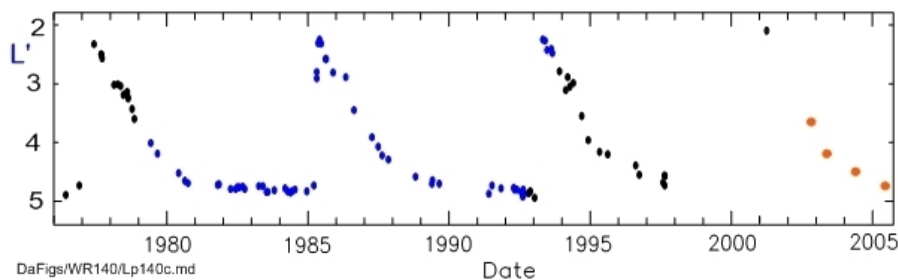


Figure 1: Long-term light curve of WR 140 in  $L'$  ( $3.8 \mu\text{m}$ ) from photometers on UKIRT (blue points), the IRFC/TCS and other telescopes (black), or derived from images (orange). The maxima occur immediately after the 1977, 1985, 1993 and 2001 periastron passages.

was observed to fade significantly at the time of the 1977 dust-formation episode (Florkowski 1982). Fortunately, the unresolved radio emission from WR 140 allowed its position to be measured precisely, so that it was one of 20 stars observed in a programme to link the radio and optical reference frames – and observations in 1982–83 (Florkowski et al. 1985) showed the emission brightening again, ensuring further observations.

The link between these unexpected phenomena observed from WR 140 and the effects of colliding stellar winds was provided by the X-ray emission. The significance of colliding winds in massive binaries can be said to date from the recognition (e.g. Prilutskii & Usov 1976) that collision of a WR stellar wind with that from a companion OB star could be a significantly stronger source of X-rays than collision of the WR wind with the OB star itself. The WC7 and O5 winds of WR 140 are fast,  $v_\infty = 2860$  and  $3100 \text{ km}^{-1}$ , and carry  $\sim 2 \times 10^{-5}$  and  $\sim 2 \times 10^{-6} M_\odot \text{ y}^{-1}$  mass-loss respectively, giving them kinetic powers ( $0.5 \dot{M} v_\infty^2$ ) in excess of  $10^4$  and  $10^3 L_\odot$ . Of this power,  $\sim 3 \times 10^3 L_\odot$  is dissipated where the winds collide, leading to shock-heating of the plasma to  $T_{ion} > 10^7 \text{ K}$  and thermal X-ray emission. The first X-ray observation of WR 140 (Pollock 1987a, with *EXOSAT*) showed it to be exceptionally luminous in X-rays; while a survey of the WR stars observed with *Einstein* showed that the WR+O binaries were generally more luminous in X-rays than single WR stars (Pollock 1987b).

These several strands were pulled together in the multi-frequency study by Williams et al. (1990), who modelled the infrared variations in terms of the formation and dissipation of circumstellar dust and derived a high-eccentricity ( $e = 0.84 \pm 0.04$ ) orbit for WR 140 adopting the period (2900 d.) from the dust-formation episodes. They developed simple models for the radio and X-ray variations in terms of the varying circumstellar extinction through the WC7 or O5 stellar winds to the wind-collision region (WCR) as the orbit progressed.

The phenomena shown by WR 140 were soon examined in terms of colliding wind theory. Usov (1991) showed that part of the WC7 stellar wind entering the wind-collision shock between the stars could cool very efficiently, and reach a density  $\simeq 10^3$  times its pre-shock value, providing cool, dense material within which dust could condense. Usov (1992) developed analytical models of the colliding winds and X-ray emission of massive binaries, and showed that the observed X-ray luminosity of WR 140 was consistent with the parameters of its winds. Non-thermal radio emission from colliding-wind binaries, and WR 140 in particular, was modelled by Eichler & Usov (1993). Stevens, Blondin & Pollock (1992) also developed models of colliding winds, drawing attention to the ratio,  $\chi$ , of the cooling to escape times of the shocked gas, which determined whether the shocks were adiabatic or isothermal. When cooling is significant, thermal instabilities in the WCR become important. On account of the separation of the stars in WR 140, the post-shock regions of its winds were considered to be close to adiabatic throughout the orbit. Under these conditions, the geometry is scale-free and X-ray luminosity should vary as  $1/D$ , where  $D$  is the separation of the stars.

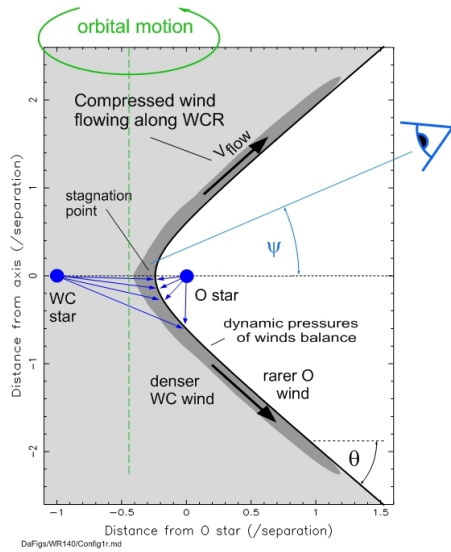


Figure 2: A slice through the WCR perpendicular to the orbital plane; the stars and WCR rotate about the vertical axis.

Theoretical work on colliding winds is becoming ever more sophisticated, as described by Pittard (2011), so a very simple model will be used here for illustration. The WCR (Fig. 2) lies where the dynamic pressures of the WC7 and O5 stellar winds balance. Its shape can be calculated from the ratio of the momenta of the two stellar winds,  $\eta = (\dot{M}v_\infty)_{O5}/(\dot{M}v_\infty)_{WC7}$ , which does not change round the orbit if the winds collide at their terminal velocities. The WCR is closer to the O5 star because its mass-loss rate and wind momentum are much lower than that of the WC star. At large distances from the stars, the WCR can be approximated by a cone (opening angle  $\theta$ ) symmetric about the axis. This is twisted to form a spiral in the orbital plane by the motion of the stars in their orbit. The pitch angle of the spiral depends on the ratio of the transverse velocity of the stars in their orbit relative to stellar wind velocities. Given the fast winds and long period of WR 140, this ratio is small but it does vary significantly (factor  $> 15$ ) near periastron, so the breadth of the spiral varies hugely round the orbit — like a badly filled sausage.

The WC7 and O5 stellar winds are shocked on each side of the WCR in regions which are wide if the shocks are adiabatic but thin and distorted by instabilities (not shown in Fig. 2) if the shocks are radiative. These shocks compress the winds, which flow along the WCR (only that of the WC7 star is shown in the figure). The compressed winds accelerate from the stagnation point on the axis (the line of centres) between the stars to reach an asymptotic value,  $V_{flow}$ , on the ‘conical’ region of the WCR, which can be calculated from the stellar winds following Cantó, Raga & Wilkin (1996). It is within the compressed, carbon-rich WC7 stellar wind that the dust is believed to condense, sufficiently down-wind to escape immediate destruction by the harsh stellar radiation. The orbital motion spreads it around in a plume whose dimensions depend on  $\theta$  and the angular movement of the WCR during dust formation. On the other hand, the X-ray emission is more likely to arise near the stagnation point, where the winds collide head-on and the post-shock temperature is highest. A goal of the observing campaigns is to use the variations to locate the different sources of emission in the WCR.

The rotation of the WCR with the stars causes our viewing angle,  $\psi$ , to vary with phase, modulating the extinction to the stars and WCR and also the observed RV of compressed wind flowing in the WCR. The angle  $\psi$  is related to the true anomaly,  $f$ , of the stars in the orbit via  $\cos \psi = -\sin i \sin(f + \omega)$ , where  $i$  is the orbital inclination and  $\omega$  the argument of periastron. If  $i$  is not known, it can in principle be determined from the variations of  $\psi$  inferred from motion of the com-

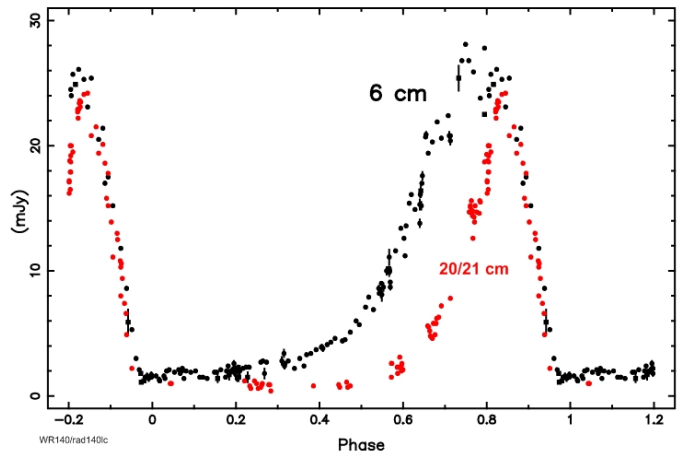


Figure 3: Phased 6-cm and 20/21-cm flux densities showing maxima well before O5 star conjunction ( $\phi = 0.95$ ).

pressed wind or varying extinction and a model for the WCR — but if we want to use the observations to study the WCR, we need an independent determination of the inclination.

The brightness of WR 140 ensured its observation with most X-ray missions: twice with *Ginga* (Koyama et al. 1990), five times with *ROSAT* before the 1993 periastron, twice with *ASCA* after the 1993 periastron, and six further observations with *ASCA* between the 1997 apastron and the radio maximum in 1999 (Koyama et al. 1994, Zhekov & Skinner 2000, Pollock, Corcoran & Stevens 2002). Like the *EXOSAT* spectra taken immediately after the 1985 periastron, the two *ASCA* spectra taken immediately after the 1993 periastron showed strong circumstellar absorption. The X-ray spectra could be reproduced with CWB shock models and reasonable wind parameters. The observations covered a sufficiently wide range of orbital phase and stellar separation,  $D$ , that it was possible to test the  $1/D$ -dependence of the X-ray flux expected from adiabatic shocks. Both Zhekov & Skinner and Pollock et al. (2002) found that the flux levels of the 1993 spectra taken near periastron were lower than expected than from the  $1/D$ -dependence and those of the other spectra, and proposed changes to the RV orbital elements – proposals not supported by existing or subsequent (Marchenko et al. 2003, hereafter MM03) orbital analyses. For the 2001 periastron passage, Pollock et al. (2005) secured *Chandra* spectra at  $\phi = 0.99$ , near X-ray maximum, and  $\phi = 0.03$ , when the flux had recovered to about half its maximum after the deep minimum near conjunction, when the WCR was observed through the densest region of the WC7 stellar wind. The flux level itself was monitored with weekly observations with *RXTE*, which showed a well defined minimum at 2001.13. The velocity widths and shifts of the spectral lines measured in the high-resolution *Chandra* spectra indicated where in the WCR they were formed and the relevant ions located. The  $\phi = 0.99$  spectrum showed blue-shifted motion of  $\sim 600 \text{ km s}^{-1}$ , while the  $\phi = 0.03$  spectrum showed red-shifted motion of  $\sim 400 \text{ km s}^{-1}$ , consistent with their formation in the accelerating wind region of the WCR (Fig. 2) and its rotation with the orbital motion.

The early radio observations were extended with WSRT observations of the 1991–92 radio maximum at 6 cm and 21 cm (Williams, van der Hucht & Spoelstra 1994) and VLA observations by White & Becker (1995) at monthly intervals around the whole orbit at 2 cm and 6 cm, together with observations at 20 cm for two years near maximum. The full light curves (Fig 3) showed that the radio maximum occurred much earlier ( $\phi \simeq 0.8$ ) than conjunction ( $\phi \simeq 0.95$ ), when the non-thermal source was viewed through the lower-density O5 stellar wind, requiring abandonment of the simple model. White & Becker developed a new model in which the wind of the WC7 star was mostly flattened into a disk inclined to the orbital plane, and this extinguished the non-thermal radio flux until the O5 star and wind-collision region (WCR) passed through it in the observer's direction. The intrinsic non-thermal emission depended on the distance from the disk, and passage through the disk near phase 0.7 accounted for the maximum intrinsic emission at that phase. This model was criticised by Pollock et al. (2002) on the basis of the X-ray observations. Also, Marchenko et al. (2003) modelled the polarization from the flattened WC7 stellar wind and showed it to be higher than the upper limits observed, unless the orientation was very contrived. *The radio flux variations remain to be explained.*

In the ultraviolet, Setia Gunawan et al. (2001) used *IUE* SWP spectra to determine the orbit of the O5 star, also adopting the 2900-d dust-formation period, and derived an eccentricity ( $e = 0.87 \pm 0.05$ ) close to that ( $e = 0.84$ ) found in the optical. The profiles of the UV resonance lines varied with phase as the sight lines to the two stars passed through different regions of the winds. In particular, absorption at velocities up to  $400 \text{ km s}^{-1}$  higher than  $v_\infty$  were observed near periastron, possibly due to observation through a turbulent region of the wind or the WCR. These results should be re-examined using the latest RV orbital elements to help determine the location of the high-velocity absorption.

For their determination of the RV orbit, MM03 observed over 100 new spectra of WR 140. They derived the first RV period, 2899 d., in good agreement with the dust-formation period (2900 d.), and

a higher eccentricity ( $e = 0.881$ ) than previous solutions. They observed the appearance of sub-peaks on the low-excitation 5696-Å C III and 5876-Å He I emission lines near periastron ( $\phi \sim 0.995$ –1.015), similar to those shown by shorter period WR+O systems with circular orbits like WR 79 (Lührs 1997). The sub-peaks were blue-shifted before periastron and red-shifted afterwards, consistent with formation in the compressed He- and C-rich WR stellar wind flowing at  $V_{flow}$  in the WCR, and its rotation with the stars in their orbit (Fig. 2). MM03 used these variations and a Lührs model of the WCR to determine  $V_{flow}$  and  $i$ . The flux in the sub-peak varied rapidly with phase, and more steeply with stellar separation than the  $1/D$ -dependence expected from optically thin emission from shocked gas in an adiabatic WCR. This led MM03 to suggest that the shock conditions switched from adiabatic to radiative for a short time around periastron.

A stronger sub-peak was observed on the flat-topped emission profile of the 1.083- $\mu$ m He I line between phases 0.96 and 1.019 (Varricatt, Williams & Ashok 2004). This also moved from the blue to the red part of the profile as WR 140 went through periastron and the RVs were consistent with a Lührs model with  $V_{flow}$  calculated from the stellar winds following Cantó et al. (1996). Varricatt et al. measured the radiative fluxes in the sub-peak to be  $\sim 10^{-13}$  Wm $^{-2}$  near periastron, and pointed out that this was a significant coolant, exceeding the X-ray fluxes,  $\sim 2.5 \times 10^{-14}$  Wm $^{-2}$  observed with EXOSAT (2–6 keV) and ASCA (1–10 keV) shortly after the 1985 and 1993 periastron passages, and supported the departure from adiabatic conditions near periastron.

The most recent radio and infrared observations have been direct imaging of the non-thermal radio emission and circumstellar dust.

Dougherty et al. (2005) imaged the non-thermal radio emission during  $\phi = 0.74$ –0.95 with the VLBA, observing a bow-shaped ridge of emission identified with non-thermal emission from the WCR. This was observed to rotate clockwise on the sky. The axis of symmetry was taken to represent the axis of the WCR projected on the sky, with the open end of the bow giving the position angle (P.A.) of the O5 star relative to the WC7 star. From this motion, the RV orbit from MM03 and the P.A. of the stars observed by Monnier et al. (2004) at  $\phi = 0.297$ , Dougherty et al. derived the orbital inclination,  $i = 122^\circ$ , and longitude of ascending node,  $\Omega = 353^\circ$ , thereby completing the definition of the orbit in three dimensions. They also used the stellar separation measured by Monnier et al. and the orbital parameters to derive a distance of 1.85 kpc to WR 140.

The dust emission from WR 140 was first imaged in 2001 ( $\phi = 0.039$  and 0.055) by Monnier, Tuthill & Danchi (2002) with the Keck telescope. More images were observed between 2001 and 2005 ( $\phi = 0.06$ –0.56) in a multi-site campaign by Williams et al. (2009) at wavelengths between 2.2  $\mu$ m and 12.5  $\mu$ m; as the dust cooled, it was necessary to observe it at longer wavelengths. The dust features were observed to expand at constant rates. Extrapolation back to the star gave ‘start’ times very close to the 2001 periastron. The deepest long-wavelength images showed faint dust features at the same position angles as the brightest dust features from the 2001 dust, but at greater distances, consistent with their formation during the 1993 periastron and subsequent movement with constant proper motion. Relation of the dust maps to the projected orbit is difficult. After deriving the complete orbit, Dougherty et al. (2005) noted that the O5 star and base of the WCR were NW of the WC7 star at the time of periastron, and commented on the paucity of dust in that direction. Owing to the high orbital eccentricity, however, the position angle of the WCR changes very rapidly around periastron passage (e.g. the P.A. of the O5 star relative to the WC star moves through *three-quarters* of its orbit in only 0.04P), accounting for the spreading of the dust around much of the orbit despite the short duration of dust formation — nucleation occurred for only  $\simeq 0.025$  P. The detailed comparison of the dust images, photometry and orbit give information on the azimuthal distribution (leading vs. following edge in the orbital plane) of matter in the WCR (Williams et al. 2009), but need re-examination with the new orbital parameters derived in the Campaign.

Table 1: Critical orbital phases and their dates in 2008–2009.

| Phenomenon                     | Phase | JD       | Date        |
|--------------------------------|-------|----------|-------------|
| Conjunction: O5 star in front  | 0.956 | 245 4719 | 2008 Sep 9  |
| Quadrature                     | 0.996 | 245 4834 | 2009 Jan 2  |
| Periastron                     | 0.000 | 245 4846 | 2009 Jan 14 |
| Conjunction: WC7 star in front | 0.003 | 245 4855 | 2009 Jan 23 |
| Quadrature                     | 0.038 | 245 4956 | 2009 May 4  |

## 1.1 The need for an intensive observing campaign

These different studies drew on and illustrated the value of WR 140 as a laboratory of wind-collision phenomena. Many other systems show one or more of the trademark wind-collision effects: X-rays, non-thermal radio emission or dust formation. These include well known systems such as WR 19, WR 125, WR 137, WR 146 and WR 147 and newly discovered WR stars in massive, obscured clusters. The presence of one or more of these observable effects in some systems has led to their consideration as CWBs (e.g. the WR stars in Westerlund 1 proposed as binaries from their X-ray emission by Skinner et al. 2006). These systems are fainter and more difficult to observe than WR 140, which is the prime target for detailed observations of wind-collision effects at all wavelengths. Another advantage of WR 140 is its proximity, which has allowed the orbit to be determined in three dimensions and the distribution of dust to be compared directly with the orbit.

Generally, the wind-collision effects show maximum activity around the time of periastron when the stars are closest and the pre-collision density of the stellar winds is greatest. At the same time and shortly afterwards, between periastron and conjunction (critical phases are given in Table 1), the circumstellar extinction to the WCR is greatest because of the orientation of the orbit. Accurate knowledge of the configuration at the time of an observation, whether for planning or interpreting an existing observation, is always important but especially in WR 140 around periastron, because the configuration changes so quickly. The eccentricity is so high that a small uncertainty in the orbit can make a significant difference to the stellar configuration on a particular date.

In preparation for the 2009 periastron, a number overlapping groups prepared observing campaigns. The goals can be divided into three categories, although the division between the second and third is artificial and should vanish as more sophisticated models are developed:

- Refinement of the orbit
- Determination of the geometry of the WCR
- Determination of physical conditions in the WCR

To tackle the problem of rapidly changing configurations, intensive observations, often daily, were sought to capture rapid changes in observable wind-collision phenomena. First results were reported at a workshop<sup>1</sup> held at Convento da Arrábida in 2010 May-June

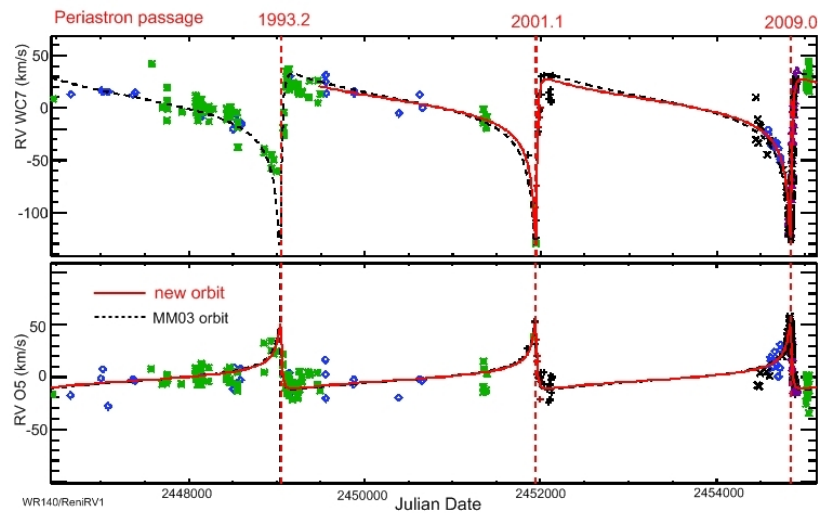


Figure 4: Three orbital cycles of RV observations showing critical requirement for intensive coverage of periastron passage and its achievement in the 2009 Campaign (adapted from Fahed et al. 2011)

## 2 Refinement of the Orbit

### 2.1 Radial velocity orbit

The first determinations of the RV orbit of WR 140 used available observations, and the study by MM03 included many more observations to provide good coverage around the orbit, but it was evident from the RV curves (Fig. 4) that the periastron passage required more intensive observations. Accordingly, Tony Moffat and Thomas Eversberg organized an observing campaign drawing on professional and amateurs. The advantage of the multi-site nature of the campaign was demonstrated when spectra were observed at the Three Hills Observatory in Cumbria (a relatively wet part of England), while poor weather was preventing observations at the usually better site on Tenerife. All the data were reduced in a consistent way and a new orbit derived by Fahed et al. (2011). The new orbital elements (Table 2) differ from those derived by MM03 in having a slightly shorter period, higher eccentricity, lower  $K_{WC}$ , and smaller uncertainties on all elements. The change in  $e$  looks small, but it makes a significant difference to the configuration near periastron, e.g. a change of  $9^\circ$  to the true anomaly at  $\phi = 0.01$ . This feeds through to comparable changes in the viewing angle,  $\psi$ , and the projected position angle of the stars at critical phases, significantly affecting the interpretation of observations. For dates near 2009, the changes in  $P$  and  $T_0$  work in opposite senses, so phases are smaller by less than 0.001 for a given date, but the differences are greater for earlier observations. The RV orbital parameters underpin the interpretation of all the other observations.

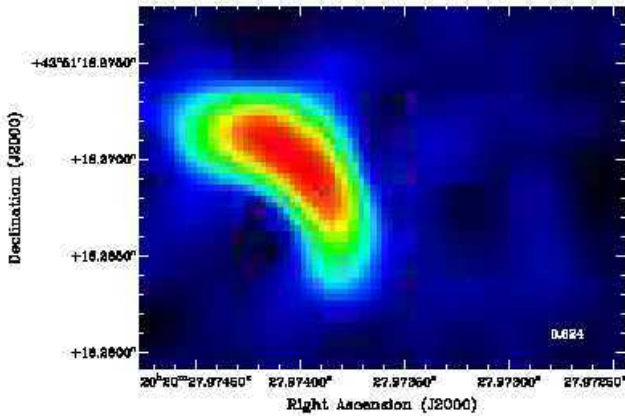
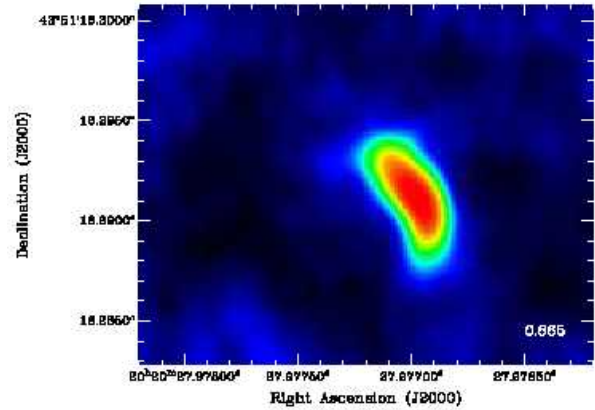
### 2.2 Astrometric orbit from radio images

Dougherty, Trenton & Beasley (2011) continued the VLBA imaging of the radio emission from WR 140, extending the phase coverage to  $\phi = 0.43\text{--}0.96$ . Two of the new 8.4-GHz images are shown in Figs 5 and 6. They show the bow-shaped emission consistent with a source in the curved region of the WCR, and comparison of the two shows both proper motion of the WR 140 system and rotation of the emission, taken to be rotation of the axis of the WCR projected on the sky. As before, Dougherty et al. used the P.A. of the stars observed at  $\phi = 0.297$  by Monnier et al. (2004) together with the

<sup>1</sup><http://astrosurf.com/joseribeiro/e.arrabida.htm>

Table 2: The RV orbital elements of WR 140

|                       | Fahed et al. (2011) | MM03                |
|-----------------------|---------------------|---------------------|
| Period (d)            | $2896.52 \pm 0.70$  | $2899.0 \pm 1.3$    |
| eccentricity          | $0.8962 \pm 0.0015$ | $0.881 \pm 0.005$   |
| $T_0$ (JD)            | $2446156.2 \pm 2.2$ | $2446147.4 \pm 3.7$ |
| $\omega$ ( $^\circ$ ) | $44.6 \pm 1.1$      | $46.7 \pm 1.6$      |
| $K_{O5}$ (km/s)       | $-30.87 \pm 0.58$   | $-30.5 \pm 1.9$     |
| $K_{WC}$ (km/s)       | $75.48 \pm 0.73$    | $82.0 \pm 2.3$      |


 Figure 5: VLBA image of WR 140 observed at  $\phi = 0.62$  from Dougherty et al. 2011

 Figure 6: VLBA image observed at  $\phi = 0.87$ 

P.A.s measured from the axes of symmetry of the bow-shaped sources to determine the inclination,  $i = 120^\circ$ , and longitude of ascending node,  $\Omega = 352^\circ$ . Comparison with the separation observed by Monnier et al. with the parameters allowed refinement of the distance to 1.81 kpc.

These results are close to those found previously, and still depend on the single interferometric observation of the stars by Monnier et al. (2004). Further such observations, which have been taken, will strengthen the results. Direct comparison of the stellar position angles with the radio images will provide a valuable test of the location of the non-thermal radio emission in the WCR, including examination of its symmetry about the axis (e.g. leading vs following edges) in the orbital plane.

With the geometric distance, extinction  $A_V = 2.9$  (Morris et al. 1993), equivalent to  $A_v = 3.2$ , and the O5 star 0.6 mag. brighter than the WC7 star in this wavelength region (van der Hucht 2001), we have  $M_v(O5) = -6.9$  and  $M_v(WC7) = -6.3$ . The luminosity and radius of the O5 star can be determined by fitting  $M_v(O5)$  with the 5160-Å flux from a 35-kK WM-Basic model appropriate to an O5 star (Smith, Norris & Crowther 2002), which gives  $R(O5) \simeq 35 R_\odot$  and  $\log(L/L_\odot) = 6.20$ . Fitting the flux from the WC7 star to a 70-kK CMFGEN model flux (Smith et al.) gives  $\log(L/L_\odot) = 5.73$ . The luminosity of the O5 star is very close to that adopted by Pittard & Dougherty (2006) but that of the WC7 star is greater by 0.23 dex. Both are rather luminous for their spectral types (cf. Repolust, Puls & Herrero 2004 and van der Hucht 2001 respectively), suggesting that the O5 star is a supergiant, and strengthening the view that the WC7 component is an unusual WC7 star. The complete orbit has  $a = 12.6$  AU and  $D$  ranging from 1.3 AU at periastron to 23.9 AU at apastron. Colliding wind theory gives the distance,  $r_{O5}$ , of the WCR from the O5 star in terms of the wind-momentum ratio,  $\eta$ :  $r_{O5} = \sqrt{\eta}/(1 + \sqrt{\eta})D$ . For  $\eta = 0.1$ , this gives  $r_{O5} \simeq 0.24D$  which, at periastron, is only 2.2  $R(O5)$ , probably too close to allow the O5 wind to have accelerated to its terminal velocity

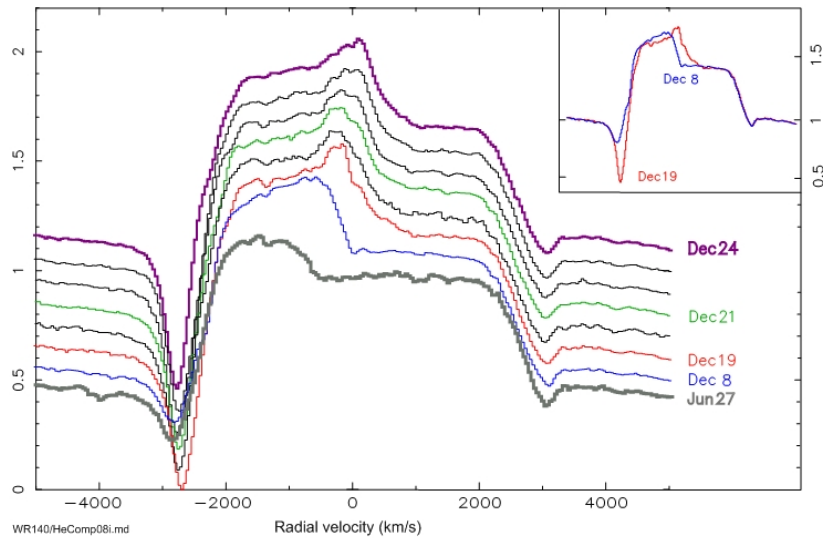


Figure 7: Profiles of 1.083- $\mu\text{m}$  line on 2008 Jun 27, Dec 8 and nightly Dec 19–24. Inset: Dec 8 and 19 spectra overplotted to show abrupt change of absorption component between these dates.

before reaching the WCR, making for a smaller WCR located even closer to the O5 star.

In reply to the question “Are we there yet?” regarding the orbit, we can answer that we are very close to having a secure orbit with all parameters — which could be nailed down with an astrometric orbit from interferometric measures of the stars.

### 3 Geometry of the Wind-collision region

#### 3.1 The absorption component of the 1.083- $\mu\text{m}$ He I line profile

Whatever the detailed structure of the WCR, it separates two stellar winds of different chemical composition and very different density, providing a significant contrast in absorption, especially of He and C features. Varricatt et al. (2004) used the variation of the absorption component of the 1.083- $\mu\text{m}$  He I profile with orbital phase to constrain the opening angle,  $\theta$  of the WCR ‘cone’ as a function of inclination.

For the Campaign, Varricatt, Adamson and Williams extended this work with further observations of the 1.083- $\mu\text{m}$  line. The new observations were taken during 2008 with UIST on the United Kingdom Infrared Telescope (UKIRT) at a resolution of  $200 \text{ km s}^{-1}$  and comprise five spectra extending the coverage to earlier phases ( $\phi = 0.93\text{--}0.95$ ) than Varricatt et al. and nine spectra, some at daily intervals, near  $\phi = 0.99$ , when the configuration of the binary was changing very rapidly. A selection of line profiles is presented in Fig. 7 to show the difference between that near conjunction (June; spectra observed in July and August were very similar) and during December shortly before periastron, when the profile was changing rapidly.

The strength of the 1.083- $\mu\text{m}$  absorption varies significantly (Figs 7 and 8), and most of the absorption must arise in the WC7 stellar wind. The underlying continuum comes from both the WC7 and O5 stars. The WC7 star is always seen through at least some of the WC7 wind (cf. Figs 2 and 9), the densest region near the star. It is also expected to be fainter than the O5 star in the one-micron region, so most of the variation observed in the 1.083- $\mu\text{m}$  line absorption component must come from the variation in absorption to the O5 star. When the viewing angle,  $\psi$ , is small, the O5 star is seen through its own wind only, which has one-tenth the density of the WC7 wind and a significantly lower

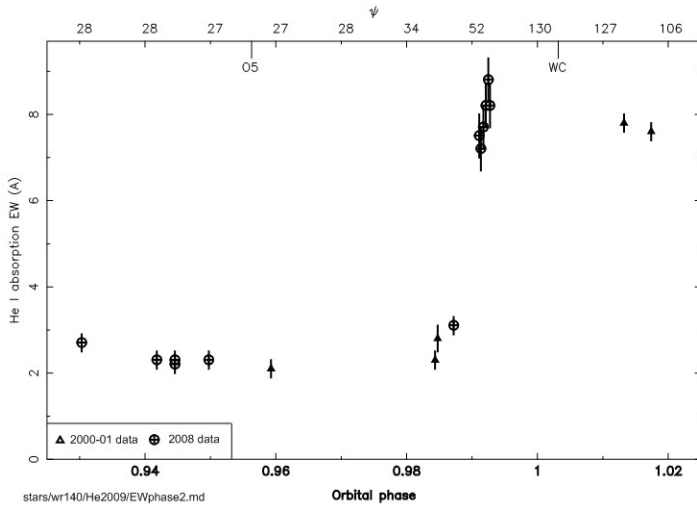


Figure 8: EW of absorption component as a function of phase near periastron. On top are the viewing angle,  $\psi$ , and phases of conjunction, ‘O5’ and ‘WC’, in front.

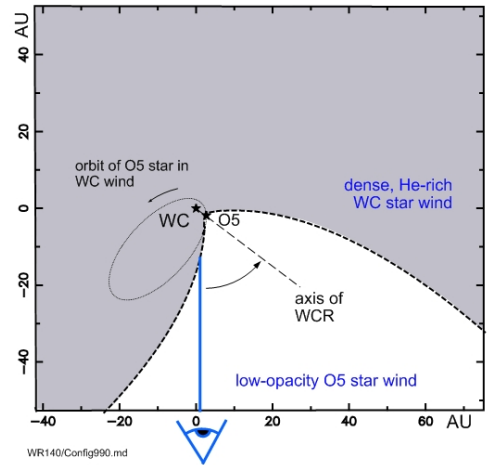


Figure 9: Sketch of the system in the plane of the orbit for the beginning of the WC7 wind ‘eclipse’ at  $\phi = 0.99$ .

helium abundance, so the absorption is at its lowest. This can be seen in Fig. 8, where the absorption is least near conjunction (O5 star in front) and barely changes while we observe the O5 star through its own wind between the first observation and  $\phi = 0.985$ , when it suddenly rises sharply. This must be the phase at which the following edge of the WCR crosses our sightline to the O5 star (Fig. 9). At this phase, the viewing angle,  $\psi$ , approaches the WCR cone angle  $\theta$ , and we begin to observe the O5 star through the more opaque WC7 stellar wind. Modelling the sharp increase of absorption (‘eclipse’) must account for the twisting of the WCR from the orbital motion, but we have a measure of the opening angle:  $\theta \simeq 40^\circ$  using the new orbital elements from Fahed et al. (2011), and  $i$  from Dougherty et al. (2011). This is  $10^\circ$  smaller than the value derived using the MM03 RV orbit and a stark illustration of the sensitivity of the configuration to the orbital elements. It implies a smaller value of the wind-momentum ratio,  $\eta = 0.05$ , locating the WCR closer to the O5 star.

### 3.2 Observations of the He I and C III line profiles

The sub-peaks observed on the  $1.083\text{-}\mu\text{m}$  He I (Fig. 7) and optical He I and C III line profiles (Fahed et al.) are believed to form in the compressed He- and C-rich WC stellar wind flowing in the WCR (MM03). The two datasets are complementary: the infrared observations cover a greater phase range ( $\phi = 0.93\text{--}1.019$ ) than the optical ( $\phi = 0.99\text{--}1.015$ ), and the sub-peaks are stronger; but the optical spectra were observed more frequently and cover crucial phases at periastron. The IR spectra were not observed often enough to pinpoint the phases at which the emission started (it was not present at  $\phi = 0.86$ ) and stopped (it had vanished by  $\phi = 0.29$ ). Fahed et al. confirmed and strengthened the result from MM03 that the flux in the  $5696\text{-}\text{\AA}$  C III subpeak varied more steeply than  $\propto 1/D$  near periastron.

Detailed comparison of the profiles of the  $1.083\text{-}\mu\text{m}$  and  $5696\text{-}\text{\AA}$  lines observed on the same dates will test whether the subpeaks are formed in the same region of the WCR. If they are, we will have relatively straightforward information on the geometry of the WCR; but if it is evident that they form in different regions, we will need models of the conditions including emissivity in the lines to identify where in the WCR they form.

In both cases, following the earlier studies by MM03 and Varricatt et al., the variations of the RVs and widths of the sub-peaks with phase were examined using the Lührs model. In this model, all the

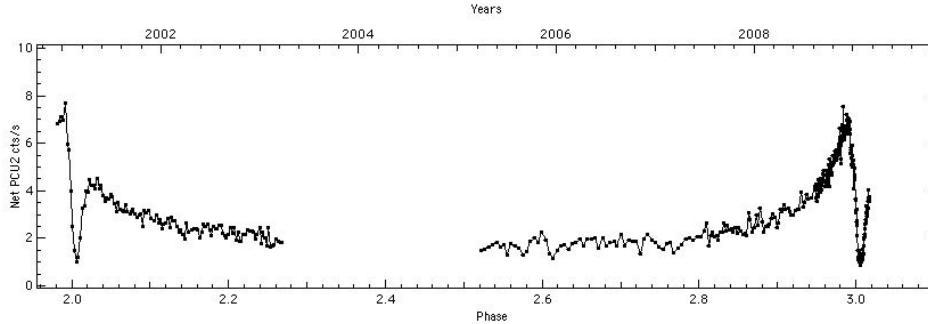


Figure 10: *RXTE* 2–10-keV count rate from WR 140 as a function of date and phase (Corcoran).

sub-peak emission arises in the ‘conical’ section of the WCR defined by the opening angle  $\theta$ , and flows with constant  $V_{flow}$ . The twisting of the WCR from orbital motion is described with a third constant ( $\delta\phi$ ), the deviation of the axis of the WCR from the line of centres of the stars. This has the virtue that it is not necessary to know the distribution of emissivity along the WCR, either radially or azimuthally around the cone: the RV and width of the sub-peak can be derived using simple analytic relations from the orbit and the model constants. The observed variations in the RVs and widths of the 1.083- $\mu\text{m}$  and 5696- $\text{\AA}$  lines were recovered, supporting their formation in the rotating WCR, but proper account has still to be taken of twisting of the WCR from orbital motion. As noted above, this depends on the ratio of the transverse velocity of the WCR to the wind velocity, which in WR 140 is small but varies significantly near periastron. The complex line profiles (Fig. 7 and Fahed et al. 2011) are not fully described by RV and line width, and require to be modelled. To date, this has not been successful with reasonable geometric parameters, and it will be necessary to consider formation over a greater range of the WCR including a ranges of angles, flow velocities and spatial variation of emissivity. The spectral sub-peaks have the promise of being a powerful diagnostic, bridging the gap between geometry and physical conditions in the WCR, especially where they can be compared with the profiles of lines observed in high-resolution X-ray spectra at the same phases.

## 4 Physical conditions in the WCR

### 4.1 Intensive X-ray monitoring with *RXTE*

For the Campaign, Corcoran et al. extended the *RXTE* Proportional Counter Array (PCA) observation set by resuming bi-weekly observations from 2005.2 (near apastron), increasing the frequency to daily from  $\phi = 0.94$  to cover the periastron. The flux curve from PCU2 is shown in Fig. 10. Matching of the two minima gives a period of 2897 d., in excellent agreement with the new RV period (Fahed et al. 2011). Comparison with a  $1/D$ -variation shows the flux falling below it between phases  $\simeq 0.93$  and 1.07. The hardness ratio was found to be constant, implying the same value of kT ( $\simeq 3\text{--}4$  keV) and collision at the same, presumably terminal velocities until near conjunction, when, from  $\phi = 0.99$ , the hardness ratio rose owing to rising extinction through the WC stellar wind. Detailed examination of the flux minimum shows that it is not wholly caused by circumstellar extinction: the *intrinsic* flux fades to a minimum near  $\phi \simeq 1.003\text{--}1.008$ . The reduced emissivity could be caused by another source of cooling or weakening of the wind collision, but the continued emission in the 5696- $\text{\AA}$  C III sub-peak through periastron (Fahed et al. 2011) argues against failure of the wind collision. Occultation is also possible as the minimum occurs near conjunction (Table 1), but probably not by the WC7 star itself given the orbital inclination.

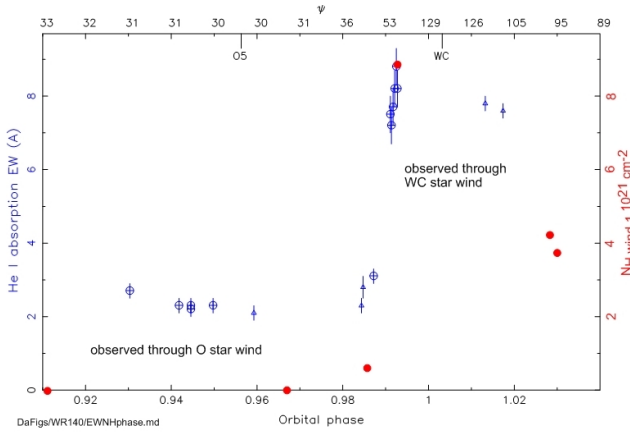


Figure 11: Comparison of onset of  $1.083\text{-}\mu\text{m}$  (blue  $\oplus$ ,  $\triangle$ ) and X-ray (red  $\bullet$ , *XMM-Newton* EPIC spectra) absorption in the WC7 wind.

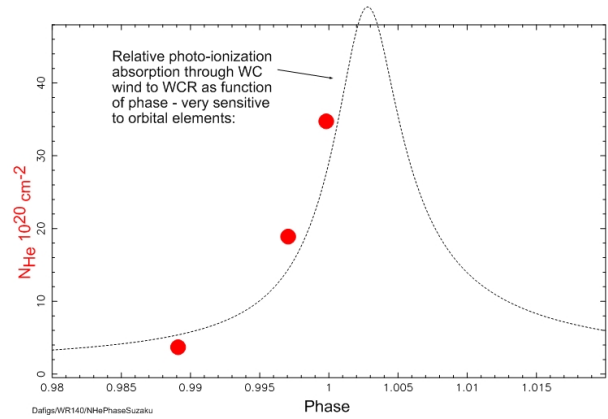


Figure 12: Inner wind extinction probed by *SUZAKU* compared with model.

## 4.2 X-ray spectroscopy using *Suzaku*, *XMM-Newton* and *Chandra*.

De Becker et al. (2011) used *XMM-Newton* to observe four spectra before periastron ( $\phi = 0.91\text{--}0.99$ ) and two afterwards ( $\phi = 1.029\text{--}1.031$ ). The  $0.3\text{--}10\text{-keV}$  EPIC spectra were fitted with three-component ( $T \sim 5, 15, \text{ and } 50 \text{ MK}$ ) thermal models giving normalisation parameters and wind extinctions for each. The normalisation parameter of the first component does not fit the  $1/D$ -dependence, e.g. rising by 5% in  $\phi = 0.987\text{--}0.994$  while  $1/D$  rises by 60%. The extinction to this component,  $N_{H,wind,1}$ , shows a rapid increase near  $\phi = 0.99$  as the sightline to the X-ray source moved from the O5 stellar wind to the WC7 wind. Fig. 11 shows  $N_{H,wind,1}$  plotted against phase, alongside the  $1.083\text{-}\mu\text{m}$  absorption equivalent widths. The similarity of the ‘eclipses’ of the X-ray source and O5 star suggests that the X-ray source is not greatly extended. The relative values of  $N_{H,wind,1}$  in the last three spectra are well fit with the absorbing column densities calculated following Williams et al. (1990) and the modern orbit (De Becker et al. 2011). The RGS spectra observed when the absorption was lower are dominated by Ne X Ly $\alpha$  and the spectra are still being analysed e.g. the *fir* ratios in the Ne IX triplet.

Sugawara et al. (2010, 2011) observed four spectra with *Suzaku* XIS and HXD-PIN at phases  $\phi = 0.90\text{--}1.00$ , giving an unprecedented view of the system at periastron. The dominant X-ray component could be fit with a  $kT \sim 3 \text{ keV}$  model with varying emission measure and circumstellar absorption. The variation of absorption with phase is consistent with expected variation (Williams et al. 1990) of wind extinction to the WCR moving in the WC7 wind (Fig. 12) but the emission measure, after rising as  $1/D$  between phases 0.903 and 0.989, then falls in the  $\phi = 0.997$  and periastron spectra. This is presumably related to the fading close to periastron seen in the *RXTE* data. Sugawara et al. attribute the fading to the failure of the O5 wind to reach its terminal velocity before collision when the stars are very close, leading to a smaller WCR and  $\theta$ . Sugawara et al. discovered two further components of the X-ray emission: a hard X-ray component observed at  $\phi = 0.989$  in the HXD-PIN ( $> 10\text{keV}$ ) band, which could be fit with a power law ( $\Gamma \simeq 1.9$  photon index), and a soft ( $E \sim 1 \text{ keV}$ ) component at phases 0.997 and periastron which was not affected by circumstellar wind absorption.

Pollock et al. observed a further high-resolution spectrum with *Chandra* ACIS at  $\phi = 0.951$ , O5 star conjunction. Its shape was very similar to that of the  $\phi = 0.65$  spectrum, differing only in intensity and wavelength shift of the lines: the profile of Ne X was blue-shifted to  $\sim -1400 \text{ km s}^{-1}$  as expected from the orientation of the WCR. The spectra should yield abundances of O, Ne, Mg and other elements in the WC wind for comparison with evolutionary models.

These studies are currently being worked up, together with others, e.g. optical photometry and

polarimetry (P.I. Moffat), *SWIFT* XRT spectroscopy (P.I. Corcoran), and radiometry at a wide range of frequencies (P.I. Dougherty). Each will shed light on conditions and processes in the wind collision in WR 140, but the goal must be the development of *consistent models able to explain all the processes together*: heating, cooling, particle acceleration, and dust formation. For example, the appearance of the sub-peak on the profile of the 1.083- $\mu\text{m}$  He I line occurs between phases 0.86 and 0.93, close to the phase ( $\phi \simeq 0.93$ ) when the X-ray emission begins to deviate from a  $1/D$ -dependence: are both these phenomena related to departure from adiabatic conditions, and is the ‘deficit’ in X-ray flux made up in IR and optical sub-peak line emission? And, closer to periastron, for about  $0.025P$ , the intrinsic X-ray flux falls, emission in the C III sub-peak reaches its maximum, and dust nucleates in the wind; are these connected? Can they be explained *simultaneously*? The multi-wavelength observations will continue to provide a fuller picture of processes in WR 140, particularly near periastron, and colliding winds in any other systems, including those for which it is more difficult to obtain such full datasets, e.g.  $\eta$  Carinae and more distant massive binaries.

## Acknowledgements

The campaign was stimulated and organized by the “Getting-to-Grips with WR 140” group comprising Andy Pollock, Julian Pittard, Kenji Hamaguchi, Mike Corcoran, Sean Dougherty, Tony Moffat, and the author. My thanks to Sean Dougherty, Rémi Fahed and Mike Corcoran for figures. I am grateful to the Institute for Astronomy for hospitality and continued access to facilities of the Royal Observatory, Edinburgh.

## References

- Cantó, J., Raga, A. C. & Wilkin, F. P. 1996, ApJ, 469, 729  
Conti, P. S., Rousset-Dupré, D., Massey, P. & Rensing, M. 1984, ApJ 282, 693  
De Becker, M., Pittard, J. M., Williams, P. M., et al. 2011, in Proceedings of the 39th Liège Astrophysical Colloquium, eds. G. Rauw, M. De Becker, Y. Nazé, J.-M. Vreux & P.M. Williams, BSRSL 80, 653  
Dougherty, S. M., Beasley, A. J., Claussen, M. J., Zauderer, A. & Bolingbroke, N. J. 2005, ApJ 623, 447  
Dougherty, S. M., Trenton, V. & Beasley, A. J. 2011, in Proceedings of the 39th Liège Astrophysical Colloquium, eds. G. Rauw, M. De Becker, Y. Nazé, J.-M. Vreux & P.M. Williams, BSRSL 80, 658  
Eichler, D. & Usov, V. V. 1993, ApJ 402, 271  
Fahed, R., Moffat, A. F. J., Zorec, J., et al. 2011, in Proceedings of the 39th Liège Astrophysical Colloquium, eds. G. Rauw, M. De Becker, Y. Nazé, J.-M. Vreux & P.M. Williams, BSRSL 80, 668  
Florkowski, D. R. 1982, in: C. W. H. de Loore & A. J. Willis, eds, Wolf-Rayet Stars: Observations, Physics, Evolution, IAU Symposium 99, 63  
Florkowski, D. R. & Gottesman, S. T. 1977, MNRAS 179, 105  
Florkowski, D. R., Johnston, K. J., Wade, C. M. & de Veigt, C. 1985, AJ 90, 2381  
Koyama, K., Kawada, M., Takano, S. & Ikeuchi, S. 1990, PASJ 42, L1  
Koyama, K., Maeda, Y., Tsuru, T., Nagase, F. & Skinner, S. 1994, PASJ 49, L93  
Lührs, S. 1997, PASP 109, 504  
McDonald, J. K. 1947, Pubs Dominion Astrophysical Obs. 7, 311  
Marchenko, S. V., Moffat, A. F. J., Ballereau, D., Chauville, J., Zorec, J., Hill, G. M., Annuk, K., Corral, L. J., et al. 2003, ApJ, 596, 1295 (MM03)  
Monnier, J. D., Tuthill, P. G. & Danchi, W. C. 2002, ApJ, 567, L137  
Monnier, J. D., Traub, W. A., Schloerb, F. P., Millan-Gabet, R., Berger, J.-P., Pedretti, E., Carleton, N. P., Kraus, S., et al. 2004, ApJ 602, L57  
Morris, P. W., Brownsberger, K. R., Conti, P. S., Massey, P. & Vacca, W. D. 1993, ApJ, 412, 324  
Pittard, J.M. 2011, in Proceedings of the 39th Liège Astrophysical Colloquium, eds. G. Rauw, M. De Becker, Y. Nazé, J.-M. Vreux & P.M. Williams, BSRSL 80, 555  
Pittard, J. M. & Dougherty, S. M. 2006, MNRAS, 372, 801  
Plaskett, J. S. 1924, Pubs Dominion Astrophysical Obs. 2, 287

- Pollock, A. M. T. 1987a, A&A 171, 135  
Pollock, A. M. T. 1987b, ApJ, 320, 283  
Pollock, A. M. T., Corcoran, M. F. & Stevens, I. R. 2002, in: A. F. J. Moffat & N. St-Louis, eds, Interacting Winds from Massive Stars, ASP Conf. Series 260, 537  
Pollock, A. M. T., Corcoran, M. F., Stevens, I. R. & Williams, P. M. 2005, ApJ 629, 482  
Prilutskii, O. F. & Usov, V. V. 1976, Soviet Ast., 20, 2  
Repolust, T., Puls, J. & Herrero, A. 2004, A&A, 415, 349  
Setia Gunawan, D. Y. A., van der Hucht, K. A., Williams, P. M., Henrichs, H. F., Kaper, L., Stickland, D.J. & Wamsteker, W. M. 2001, A&A 376, 460  
Skinner, S. L., Simmons, A. E., Zhekov, S. A., Teodoro, M., Damineli, A. & Palla F. 2006, ApJL 639, L35  
Smith, L. J., Norris, R. P. F. & Crowther, P. A. 2002, MNRAS 337, 1039  
Stevens, I. R., Blondin, J. M. & Pollock, A. M. T. 1992, ApJ 386, 265  
Sugawara, Y., Maeda, Y., Tsuboi, Y. & Hamaguchi, K. 2010, AIP Conf. Procs, 1248, 9  
Sugawara, Y., Maeda Y., Tsuboi Y., et al. 2011, in Proceedings of the 39th Liège Astrophysical Colloquium, eds. G. Rauw, M. De Becker, Y. Nazé, J.-M. Vreux & P.M. Williams, BSRSL 80, 724  
Usov, V. V. 1991, MNRAS, 252, 49  
Usov, V. V. 1992, ApJ 389, 635  
van der Hucht, K. A. 2001, New Astron. Rev., 45, 135  
Varricatt, W. P., Williams, P. M. & Ashok, N. M. 2004, MNRAS, 351, 1307  
White, R. L. & Becker, R. H. 1995, ApJ 289, 698  
Williams, P. M., van der Hucht, K. A., van der Woerd, H., Wamsteker, W. M., Geballe, T. R., Garmany, C. D. & Pollock A. M. T. 1987, in: H. J. G. L. M. Lamers & C. W. H. de Loore, eds, Instabilities in Luminous Early Type Stars, D. Reidel, 221  
Williams, P. M., van der Hucht, K. A., Pollock, A. M. T., Florkowski, D. R., van der Woerd, H. & Wamsteker, W. M. 1990, MNRAS, 243, 662  
Williams, P. M., van der Hucht, K. A. & Spoelstra, T. A. Th. 1994, A&A 291, 805  
Williams, P. M., Marchenko, S. V., Marston, A. P., Moffat, A. F. J., Varricatt, W. P., Dougherty, S. M., Kidger, M. R., Morbidelli, L., et al. 2009, MNRAS 395, 1749  
Zhekhov, S. A. & Skinner, S. L. 2000, ApJ 538, 808

## Discussion

**J. Groh:** Concerning the He I 10830 line profile, I have two questions:

1. Do you see variations in the maximum velocity of the P-Cygni absorption profile?
2. Apparently there is red shifted He I 10830 absorption at  $+3000 \text{ km s}^{-1}$ . Is that real or due to blends?

**P. Williams:**

1. No, there are no conspicuous changes in the width of the absorption component.
2. I expect it is due to the gap between the He I line and a He II line in the WR star (at the position of  $P\alpha\gamma$ ).

**S. Owocki:** Regarding the disappearance of X-rays near periastron, I would again note that the severe thin-shell instabilities that occur in radiatively cooled shocks make it essentially impossible for any numerical code (even with AMR) to give reliable X-ray fluxes, because of numerical diffusion and/or mixing of hot and cold material. But such mixing seems likely also to be physically possible in nature, and if it is efficient enough, this could effectively soften or even quench the X-rays, by shifting the radiative emission to EUV and UV from the cool or warm material. This could well be a key point of the explanation for the sharp X-ray minima in WR 146 and other eccentric wind collision systems.

**L. Oskinova:** In conjunction, when the WC star was in front, did you detect intrinsic X-ray emission from the WC star wind?

**P. Williams:** No, I don't think so.